

## FINDINGS: CAST MODULAR NODES FOR SEISMIC RESISTANT STEEL FRAMES

This report contains the findings made on NSF CMS01- for the time period ending September 30, 2000. The report is organized according to connection concept: (I) Modular Connector; (II) Modular Node; and, (III) Post-tensioned Connecting System.

### A. MODULAR SEMI-RIGID CONNECTOR FOR PRF'S

#### A.1. Analytical Results

The analytical program involved two main studies: (A) a comparison of the MC to an analogous traditional tee-stub connection; and, (B) a study of key configuration parameters.

##### A.1.a. Comparison to Traditional Tee-Stub Connection

Nonlinear finite element analyses were performed to compare the response of the modular connector to the traditional tee-stub connection. The MC used is the alpha prototype configuration described in the next section. A WT 12x52 tee-stub with 1" diameter A325 bolts at an effective gage of 2" was found suitable for comparison purposes. The two-dimensional FE model of the tee-stub was validated through comparison to full-scale experiments conducted as part of the SAC Project [Leon, 1999, Swanson et al, 2000]. The demand on both connectors at various performance levels was observed by displacing the outstanding leg and applying the necessary kinematic boundary conditions. The results show excellent agreement

The overall load versus displacement plot is shown for the MC and the bolted tee-stub (See Figure 1). This plot indicates that the MC and WT are nominally identical in stiffness and strength; however the MC does achieve greater secondary strength. This reserve strength occurs due to a more significant presence of catenary action because of the role of the base and gap on the final failure mechanism..

Figure 2 shows half-symmetry models of the traditional tee-stub detail piece and a modular connector of similar strength and stiffness. Equivalent plastic strain is shown in the contours at the identical deformation demand (0.03 rad for W33 beam: 840mm beam depth).

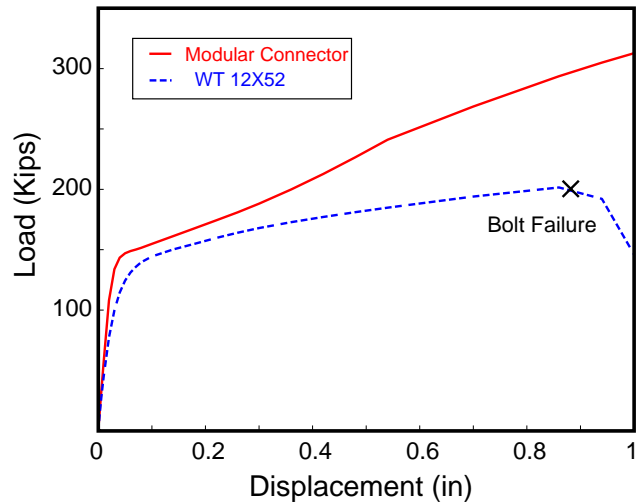


Figure 1 Load-Displacement Comparison

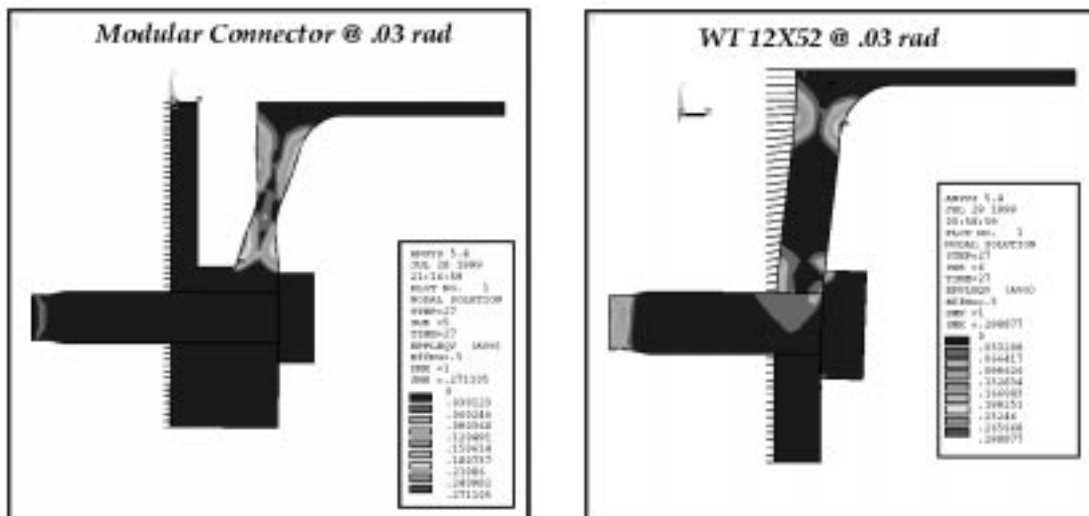
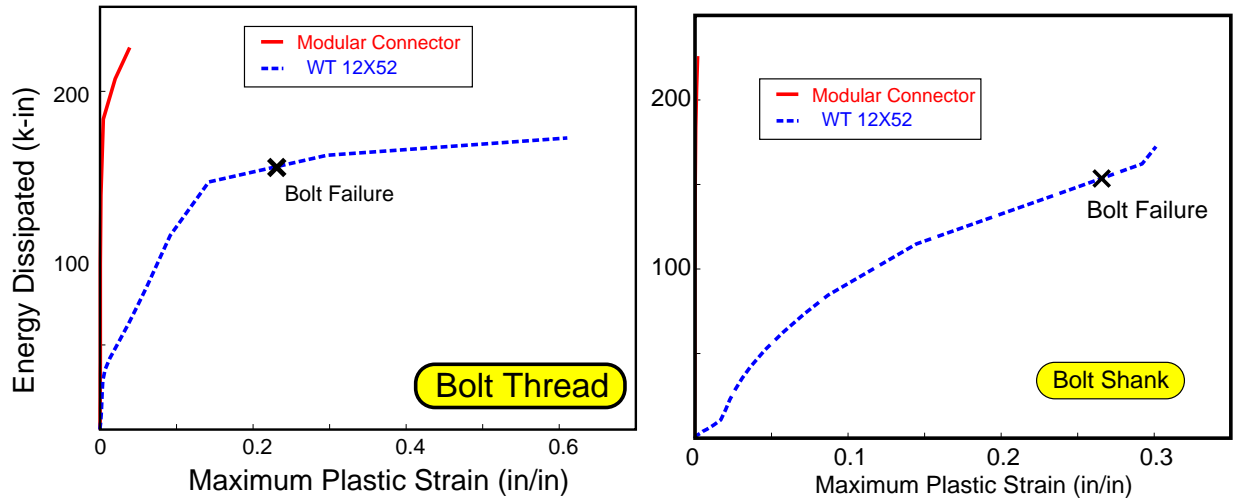
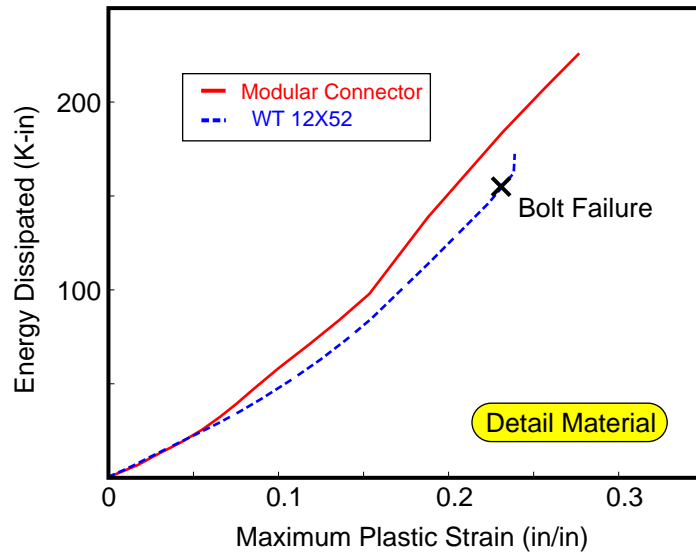


Figure 2. Plastic Strain Demand Comparison: (a) Modular Connector C; (b) Standard WT.



**Figure 3.** Maximum Plastic Strain in Bolt: (a) Threads; (b) Shank.

In comparison to the traditional tee connection, the modular connector exhibits: (1) significantly lower plastic strain in the bolt threads, shown also in Figure 3a; (2) virtually no plastic behavior in the bolt shank, shown also in Figure 3b; and, (3) lower plastic strain in the detail piece (See Figure 4). Also indicated in Figure 3a is the point at which bolt thread failure is assumed to occur [Kulak et al, 1987].



**Figure 4.** Connector Plastic Strain

Figure 5 shows the significant reduction in prying forces in the modular connector with respect to a tee of equal strength and stiffness properties. Note that the MC pre-tension is overcome at about twice the overall applied force of the tee. The rotation induced on the bolt shank at the bolt head is significant in the WT (See Fig. 15a). It is of interest to note that the prying force in the MC actually dissipates at large deflection of the MC (See Fig. 15b). This effect occurs because the contact migrates from beyond the bolt to the middle of the MC.

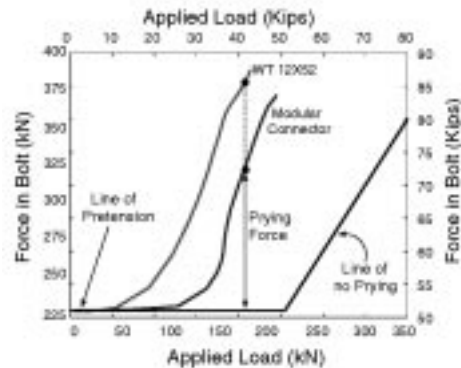


**Figure 5.** Comparison of Prying Action

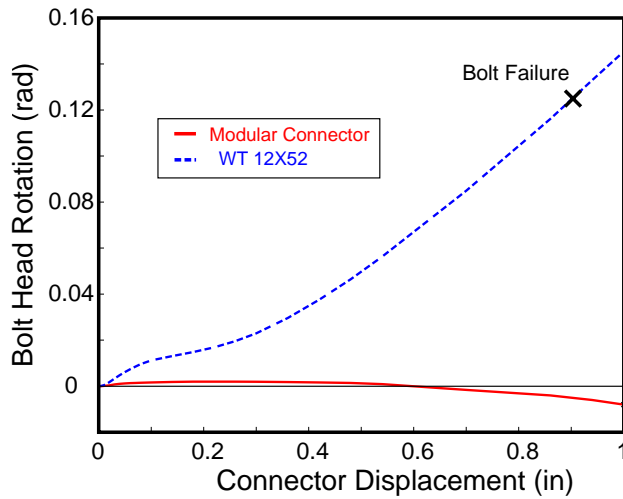


**Figure 6a.** Rotation at bolt head on shank

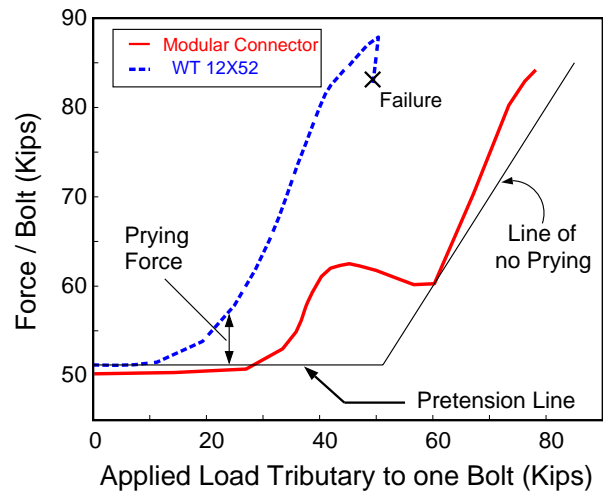


**Figure 6b.** Bolt prying comparison

### A.1.b. Evaluation of Key Configuration Parameters

Parametric studies were performed to determine the effect of connector configuration on bolt response. Two parameters are presented here: (1) base thickness, and (2) arm/base gap. These parameters do not significantly affect global response (See Fig. 7a). The base thickness was adjusted from no base to 19mm (3/4") base. As expected, increase in base thickness lowers plastic strain demand on the high strength bolt (See Fig. 7b). Similar reduction is realized in bolt prying and bending forces. The major increase in reduction takes place between configurations with no base and the configuration possessing the thinnest base. Thus, a thicker base provides minimal additional benefit. Accordingly, only a small amount of extra material is required to achieve desired behavior.

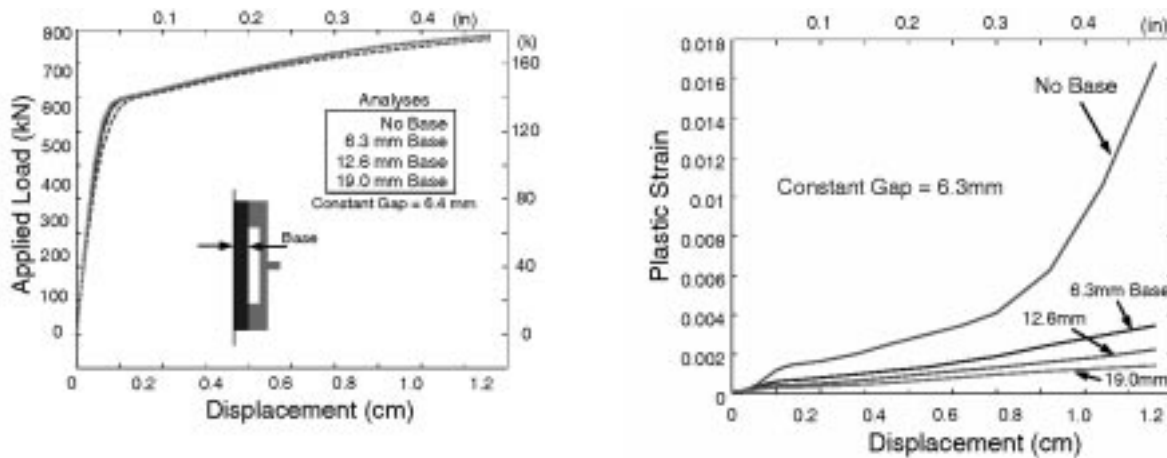


**Figure 7.** Effect of Base Size on Connector Performance: (a) global, (b) bolt response.

Not as obvious is the bolt response reduction achieved by increasing the gap between the base and the arm. Figure 8a shows the reduction of plastic strain demand in the bolt as the gap is varied. To isolate the effect, the connectors were analyzed without a base. Thus, the lower limit (zero gap) represents a traditional WT shape. A significant reduction in bolt response is demonstrated through an increase in the spacing of the gap.

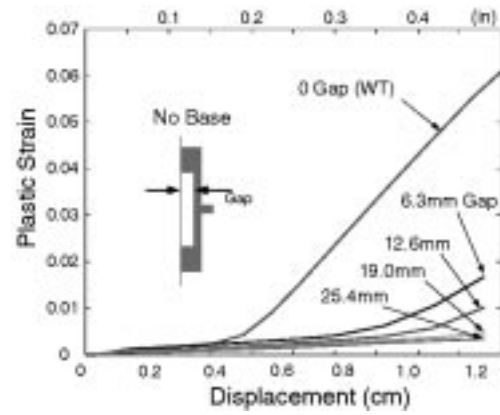


**Figure 8:** (a) Effect of Gap Size on Bolt

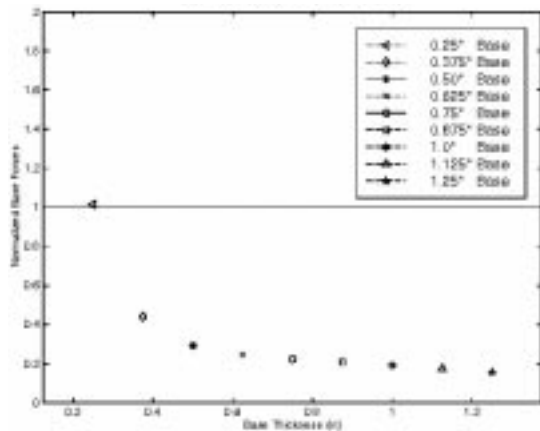


**Figure 8:** (b) Effect of Base on Force.

The compressive force associated with the size of the base was also investigated. Figure 8b shows a plot of compressive force in the base versus size of the base. As seen in the plot, the force in the base rapidly converges to a constant value, indicating that an extremely thick base is not necessarily required.

These connector details lower demand on fasteners thus allowing attainment of high connection strengths for practical bolt sizes, while mitigating poor hysteretic behavior due to loss of bolt pretension or fastener inelasticity.

## A.2. Experimental Results

The intended loading of the first test was monotonic. However, the magnitude of increased strength due to catenary action was not anticipated by the original (first-order) FE analyses. Thus, the first alpha-prototype specimen exceeded the strength of the cyclic axial-load testing fixture (220 kip). For this reason, a low-cycle fatigue (LCF) test was performed instead. The casting was cycled 13 times at 0.4" (See Figure 9) prior to a LCF failure. The subsequent large-deformation FE results shown in the figure estimates the strength accurately but overestimate the initial stiffness.

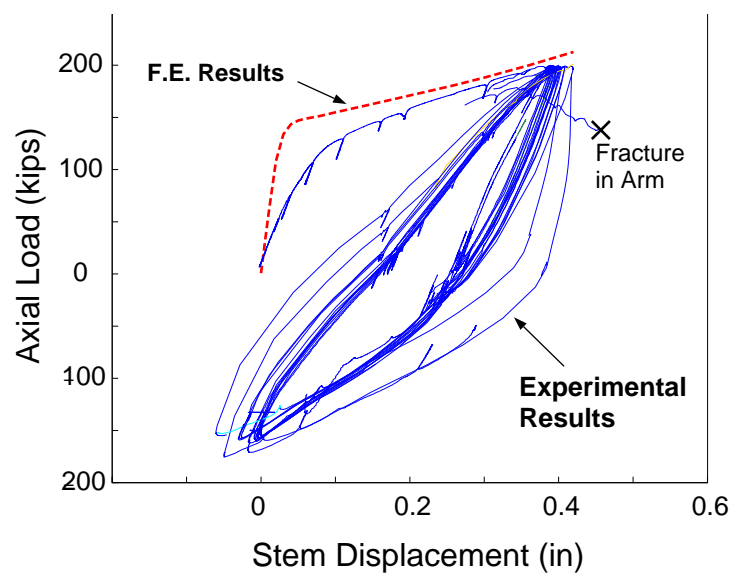


**Figure 9.** Hysteresis Curve: Alpha Prototype Experiment #1.

The LCF failure occurred in the high tensile stress region of the MC arm (See Figure 10). This region contains tension due to flexure of the arm and catenary action of the MC. Additional measurements taken during the experiments included: load, displacement, bolt force, bolt slip, bolt head displacement, bolt head rotation, and bolt shank strain. The bolt rotation was captured by placing displacement transducers (LVDT's) at the top and bottom of the head. The bolt strain was measured on the bolt shank adjacent to the bolt head at the outer and inner primary bending faces. The measured bolt rotation was about 50% of that which was predicted by FE analysis. The measured bolt strain was found to about 90% of what the FE results predicted.



**Figure 10.** Fracture of MC 1.

The alpha prototype casting did however exhibit the desired spread of plasticity engineered into the MC. The whitewashed MC permitted the observation of the plasticity spread throughout the hourglass arms (see Figure 11). This behavior was quite different from the hinge lines observed in tee-stub connector tests with connector mechanisms.

In experiments 2-4, the connectors were tested monotonically. In these tests, the width of the MC was reduced to create a specimen of ultimate strength within the capacity of the test fixture. The strength of the MC was reduced by cutting the original 9" wide specimen into 6" (tests 2,3) and 7" sections (test 4). The 7" section also had its base removed to examine the effect of the superimposed catenary forces on the failure of the connector. Each of these tests incurred specimen fracture at or near a displacement of 0.7", about half the expected 1.4" ultimate (from FE).



**Figure 11.** Spread of plastic region in MC.

To investigate possible material-related reasons for the poor performance of experiment MC 1, an ASTM 505 tensile specimen of the parent MC material was milled and tested. The tensile specimen failed at 85 ksi after undergoing only 17% elongation and only 10% reduction in area (See Figure 11). It was determined at this time that the steel used, ASTM A216 Grade WCB, had not met the performance specifications detailed by the research team, and thus was not suffi-

ciently inherently ductile for this application. The team requested that Eagle Alloy recreate the alpha prototype with a steel that meets the ductility requirements. Eagle Alloy selected 'Dynamo' steel, which is first normalized, then tempered after being poured

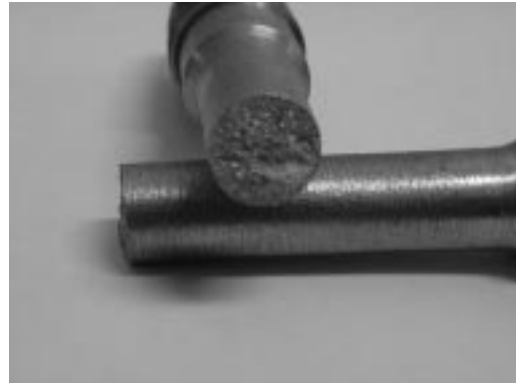
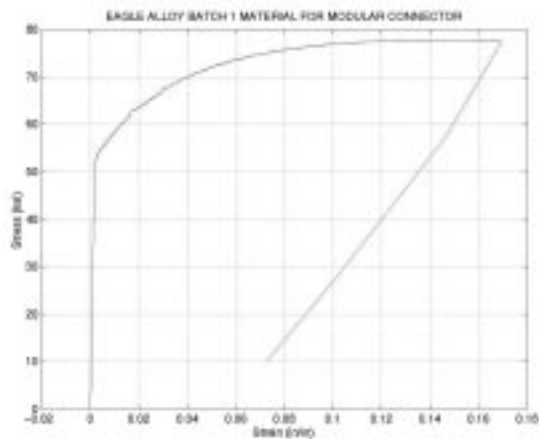


**Figure 12.** Alpha Prototype 1 Tensile Test: (a) Stress-Strain; (b) Fracture surface.

A new set of alpha prototypes were then cast with 'Dynamo' steel.

#### FRACTURE PLANES OF ALPHA PROTOTYPES

*This view shows the 3" Section that we tested.*

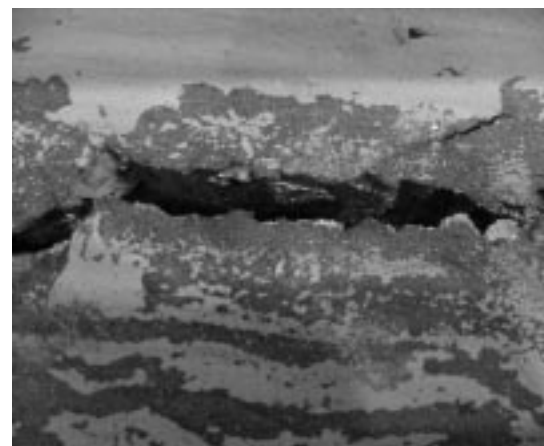
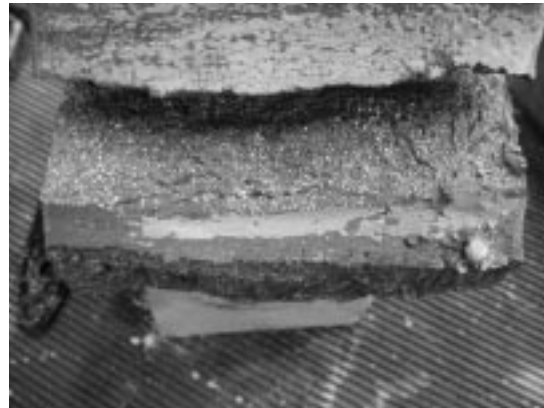
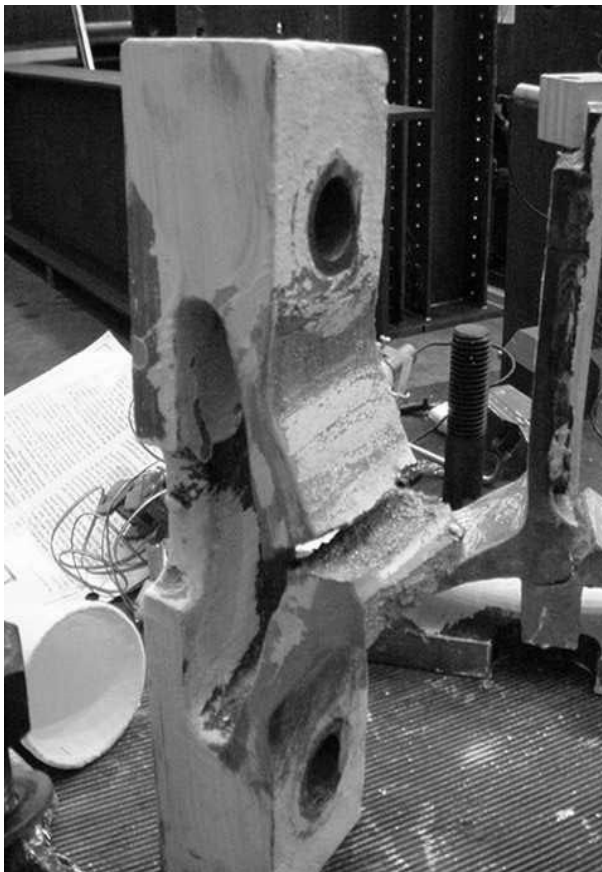


**Figure 13.** Close up of 9" section.

Often we had brittle cracks on the 3" sections and they initiated where the surface was rough as shown in this

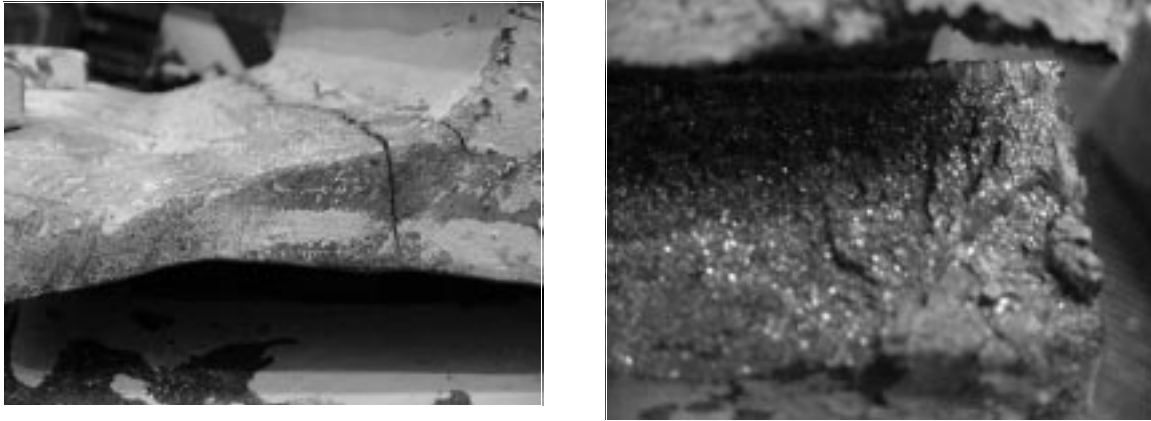


**Figure 14.**

A WT 12x52 with 1-1/8" diameter, A490 bolts was also tested. The bolts were placed at the same effective gage as the FE model of the tee-stub. The reason for the stronger bolts was to force the failure mechanism into the tee-stub, thus allowing a comparison between connectors that develop mechanisms in their principal flexural spans.

The load-displacement of the WT 12x52 is shown in Figure 15.

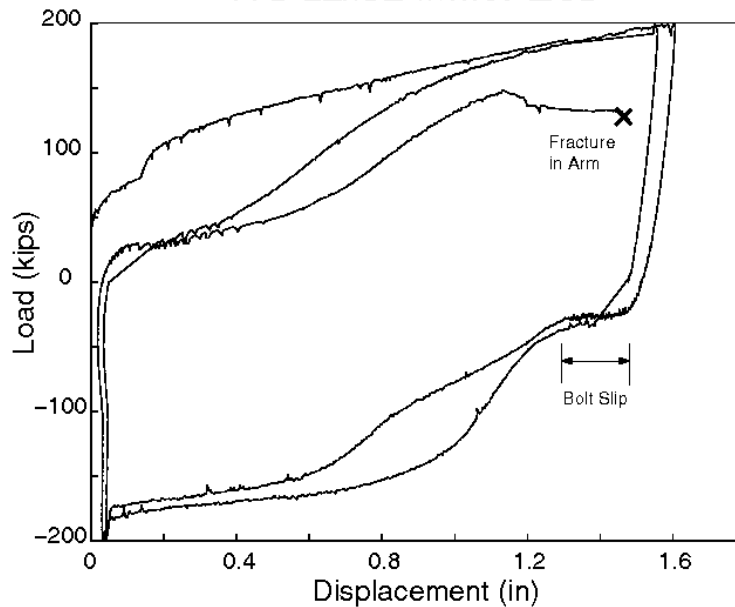


**Figure 15.**

Constraints in the set-up did not allow for the bolt slip to be measured and subtracted for this test. However, it is apparent the bolt slip accounted for about 0.2" of additional stem displacement. This test will be used for comparison to future MC tests.

## B. MODULAR NODE

### B.1. Analytical Results from Modular Node Models

Two kind of new connections were developed by now: continuous node and cruciform node. In the research, we kept those new models having the same (or close) global behaviors with the standard traditional bolted connection model and then compare the fetures listed before, we have:

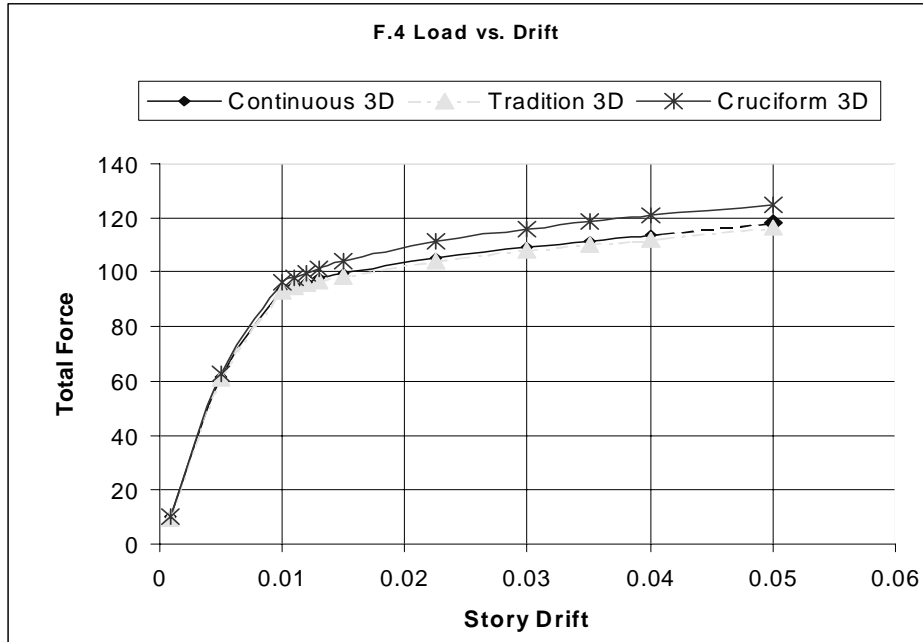


Figure 16.

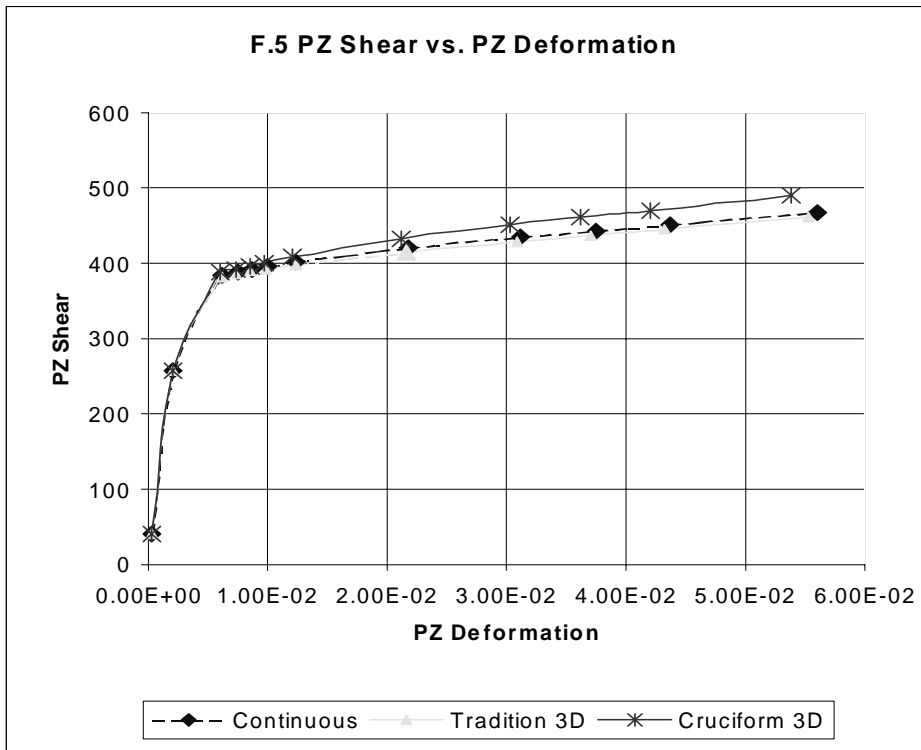


Figure 17.

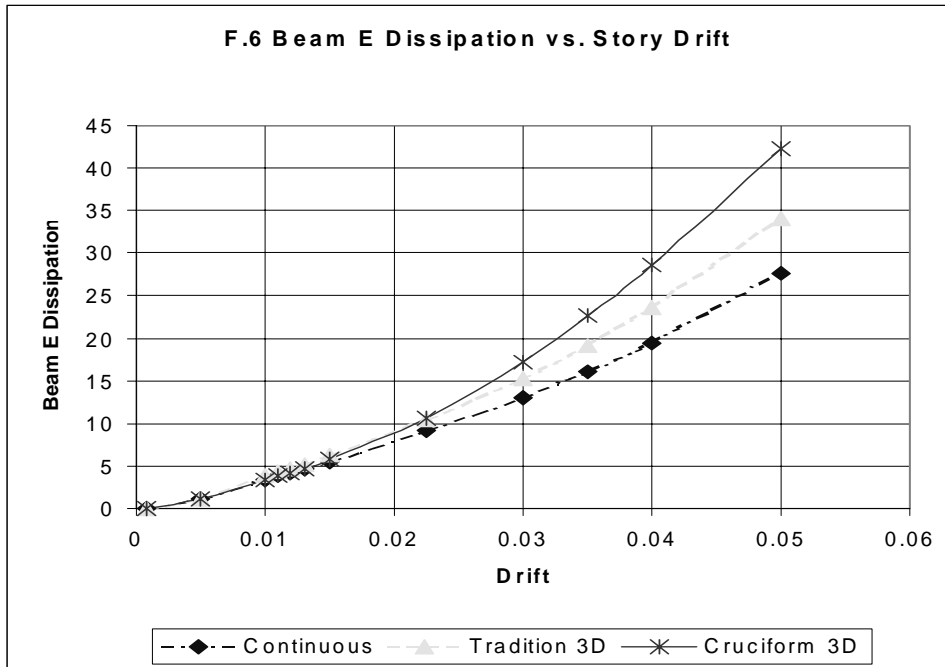
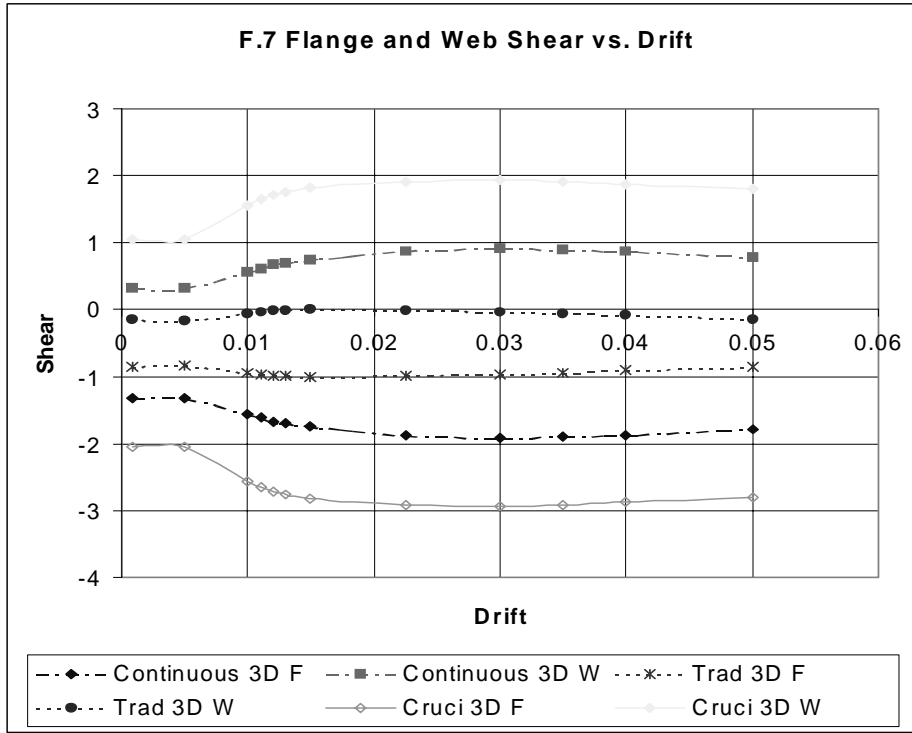


Figure 18.



**Figure 19.**

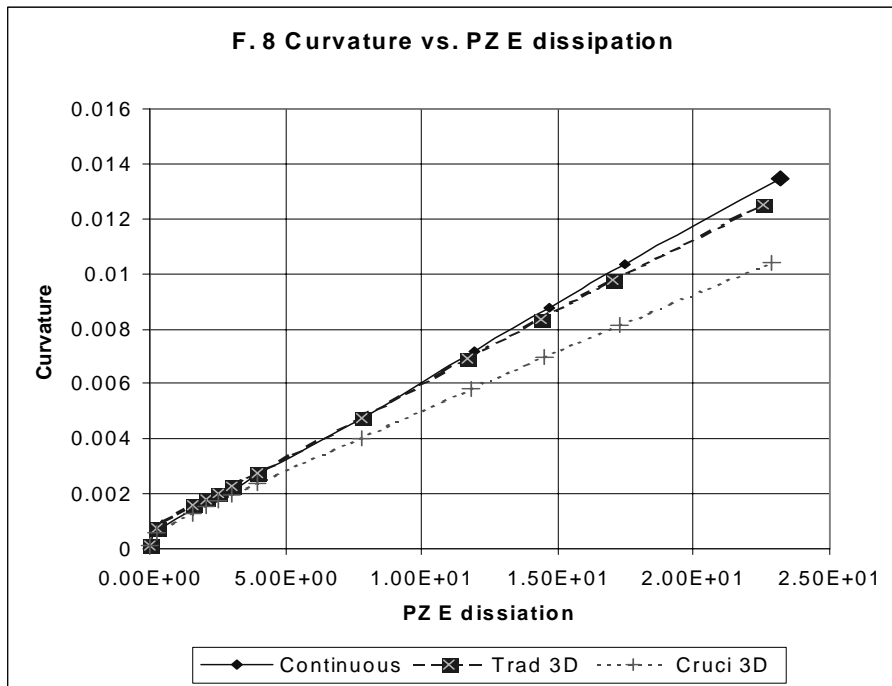


Figure 20.

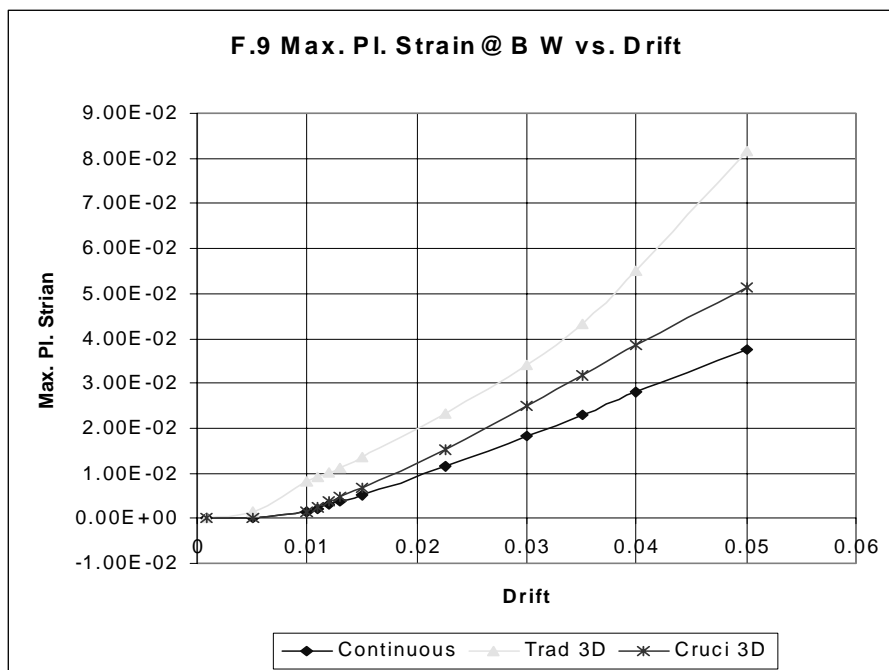


Figure 21.

We can find from these comparisons that the fetures can be improved in new connections. We'll do further research to do parametric study to find out the better geometry of new connections. An alpha-prototype design is scheduled for experimentation in September 2001.

## C. Findings from Post-Tensioned Connector Research

### C.1. Analytical Results

#### C.1.a General Behavior

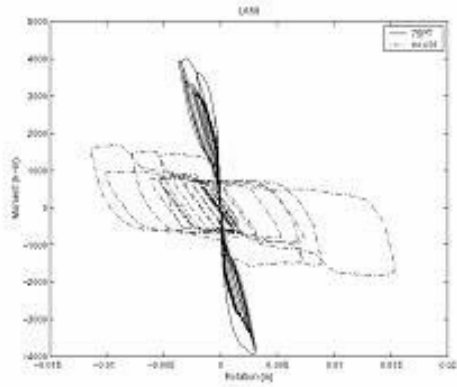


Figure 22.

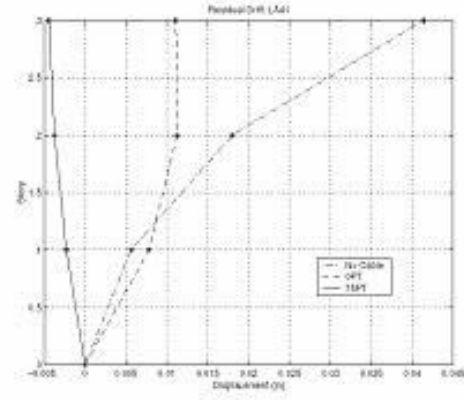


Figure 23.

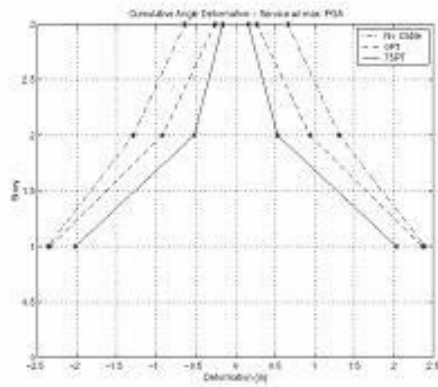


Figure 24.

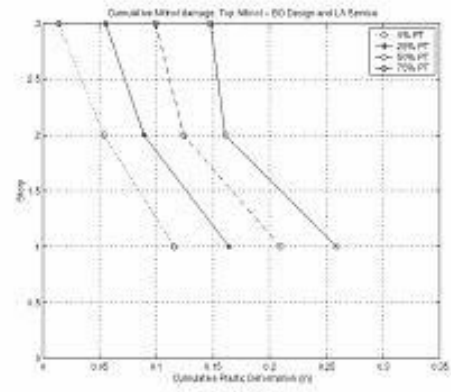


Figure 25.

Overall Response:

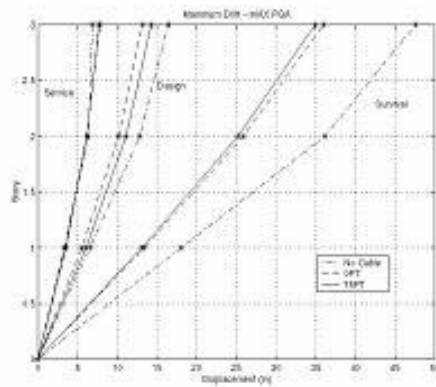


Figure 26.

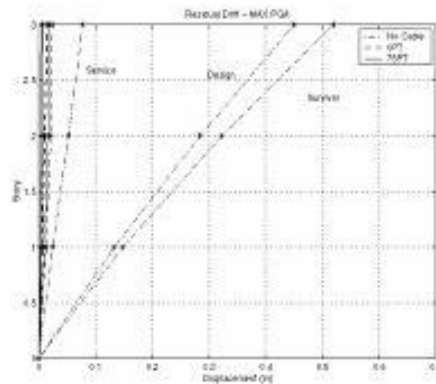


Figure 27.

### C.1.b. PT Tendon Material

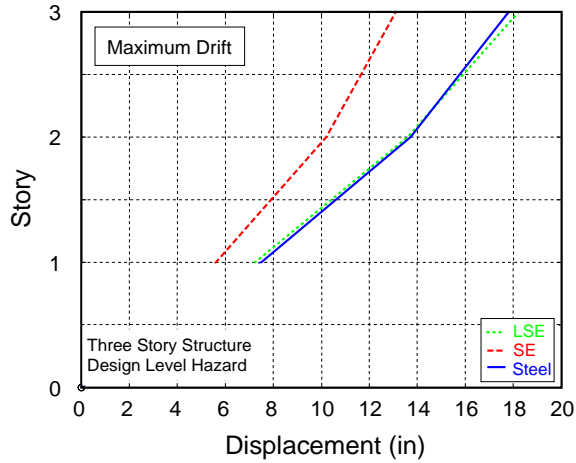


Figure 28.

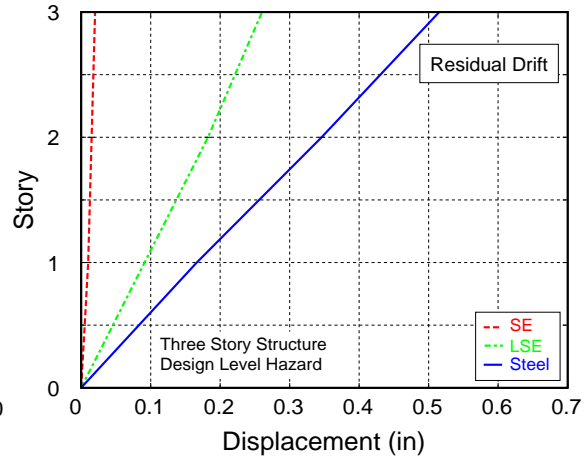


Figure 29.

### Comparison: Steel, SE Nitinol; LSE Nitinol

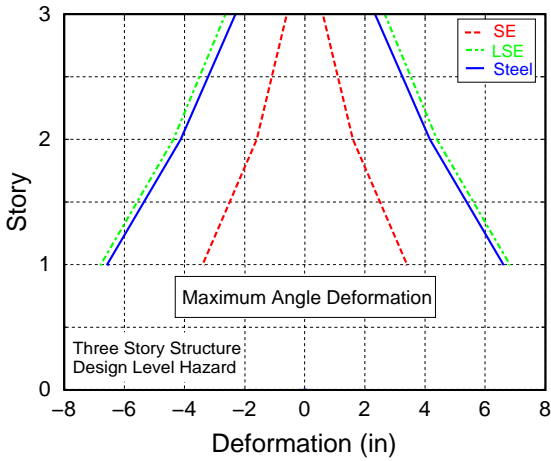


Figure 30.

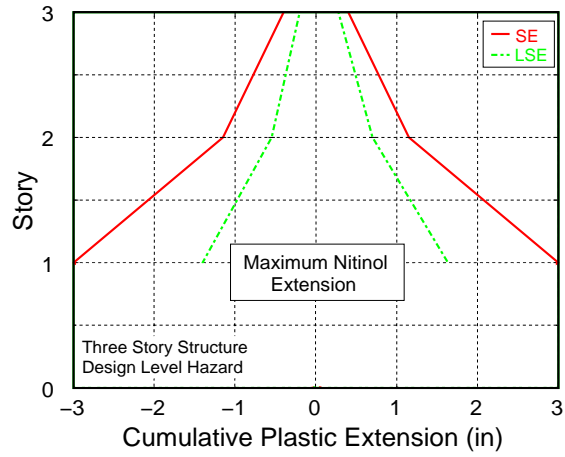


Figure 31.

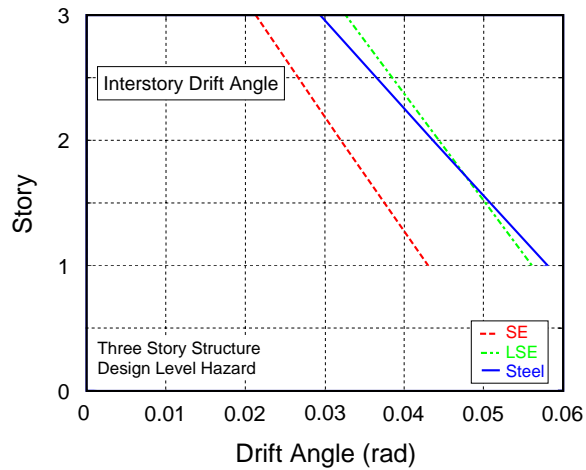
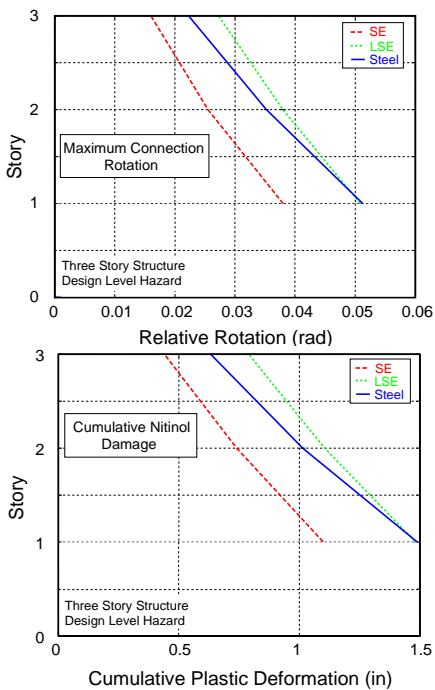


Figure 32.

### C.1.c. Service Level Response: Pretension level

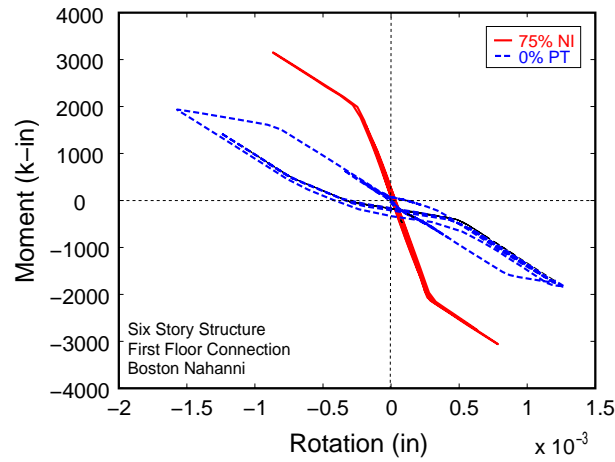


Figure 33.

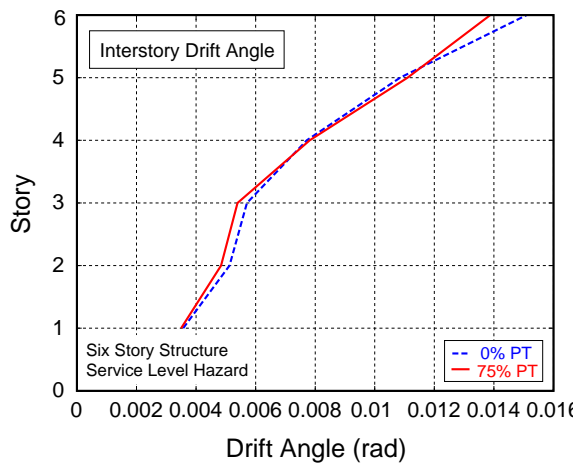


Figure 34.

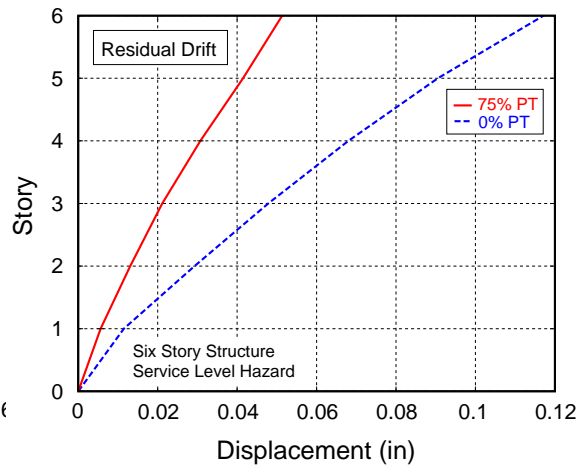


Figure 35.

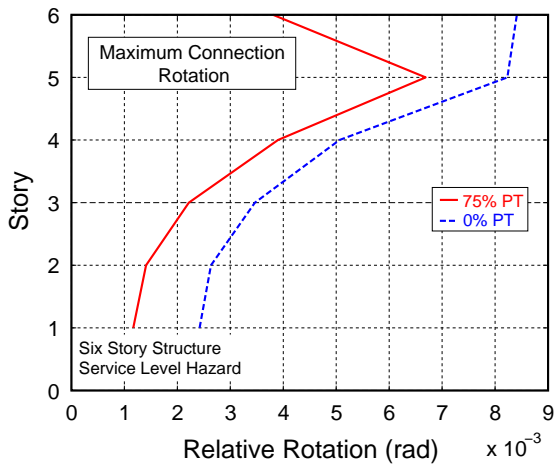


Figure 36.

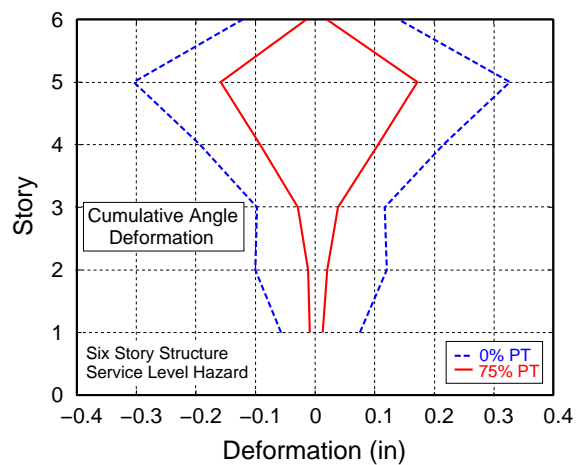


Figure 37.

### C.1.d Design Level Response: Mild vs. Restoring Ratio

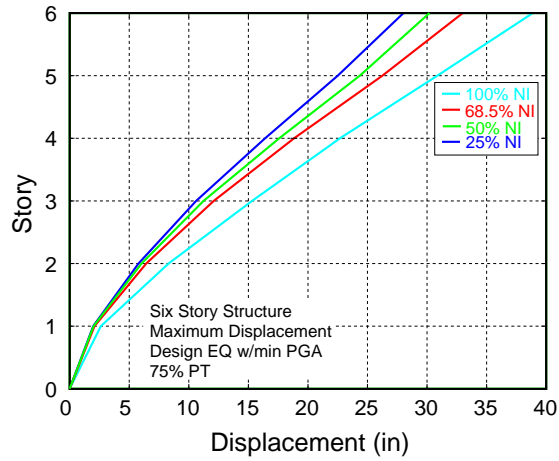


Figure 38.

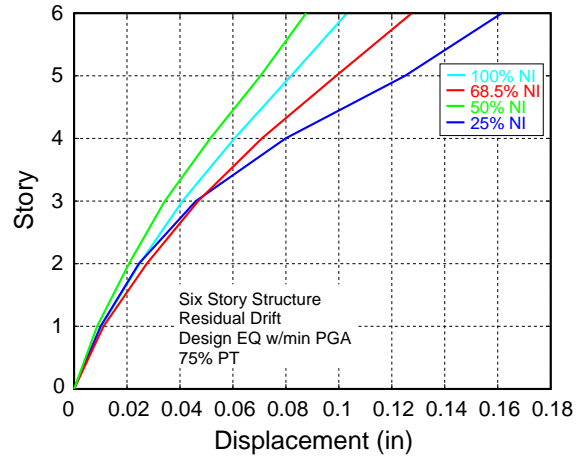


Figure 39.

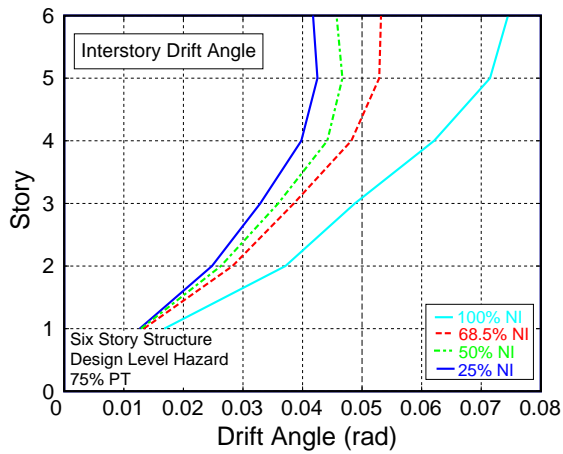


Figure 40.

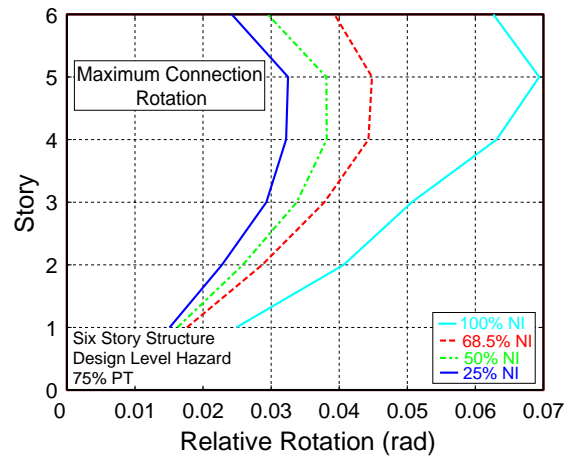


Figure 41.

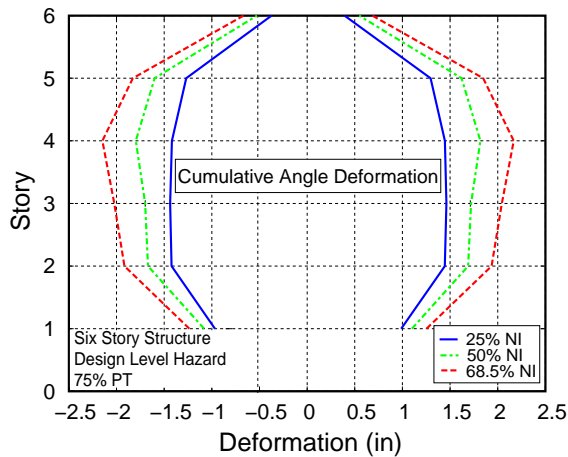


Figure 42.

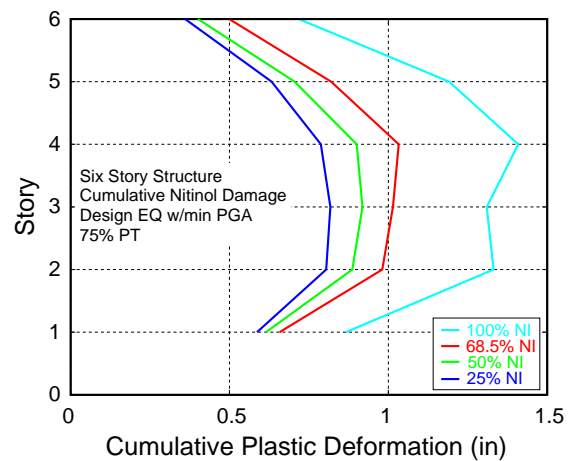


Figure 43.

### C.1.e Improvement with increasing Post-tensioning Elements

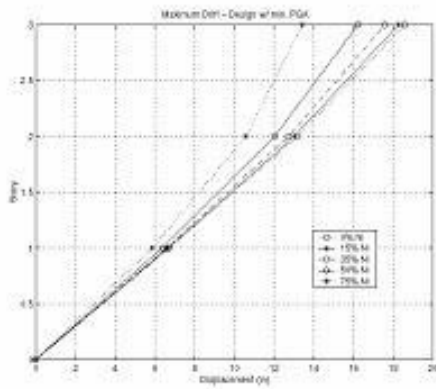


Figure 44.

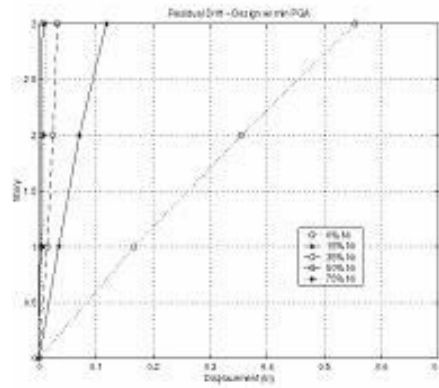


Figure 45.

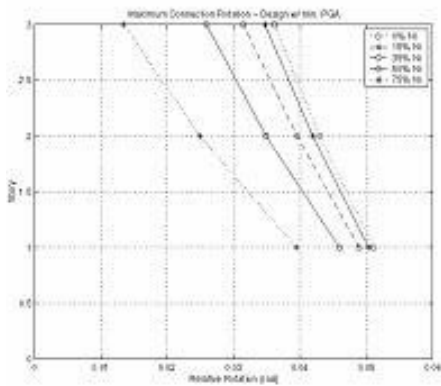


Figure 46.

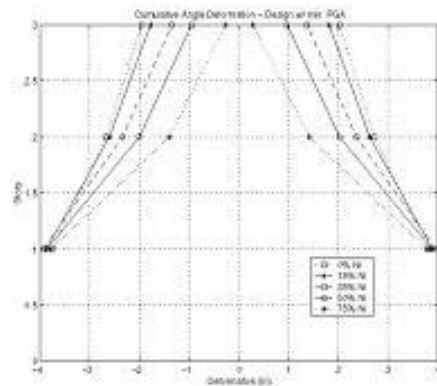


Figure 47.

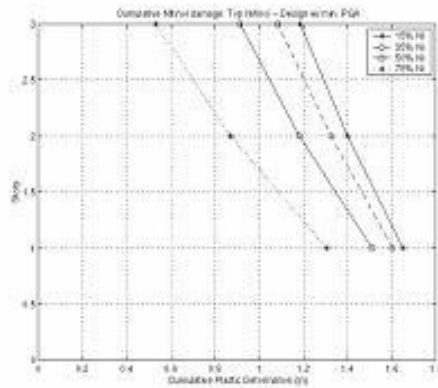


Figure 48.

## C.2 Experimental Results

### C.2.a Experimental Photographs



**Figure 49.**



**Figure 50.**



**Figure 51.**

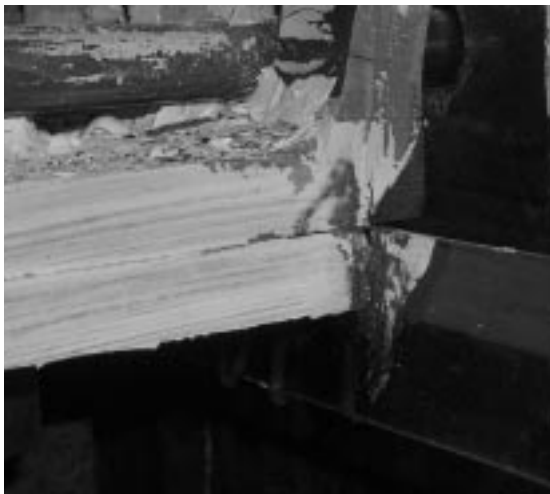


**Figure 52.**

## C.2.b Experimental Results

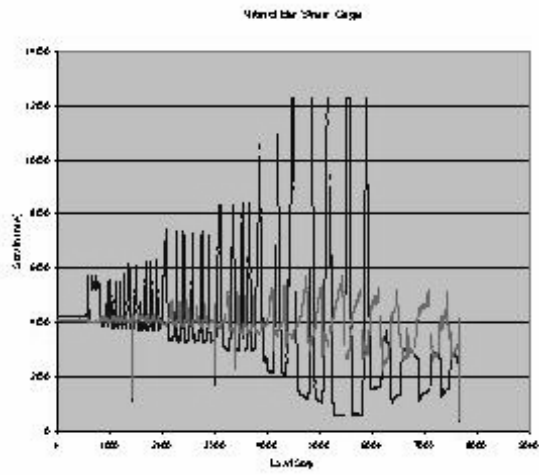


Figure 53.

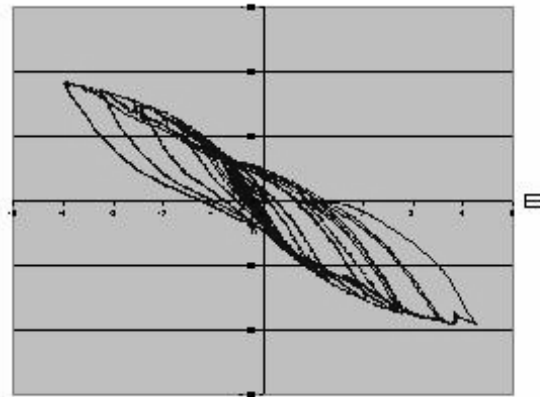


Figure 54.

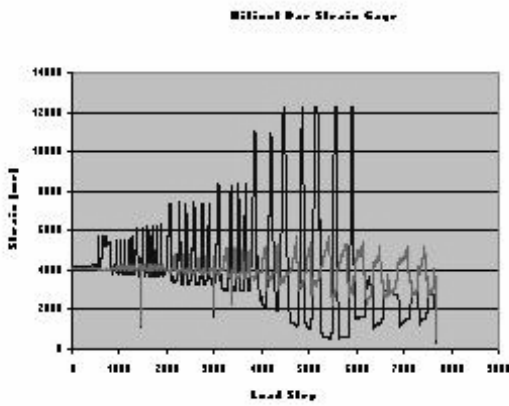


Figure 55.

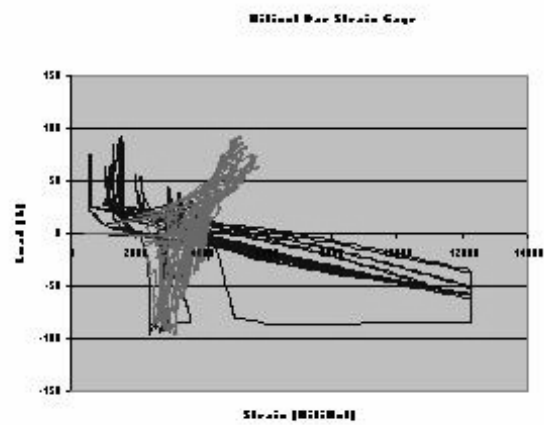


Figure 56.

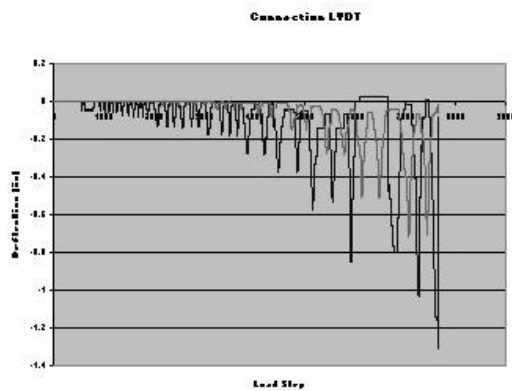


Figure 57.

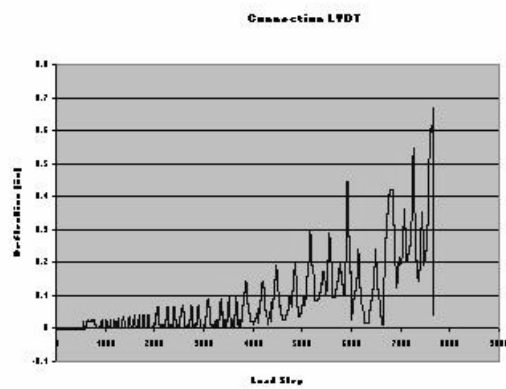


Figure 58.

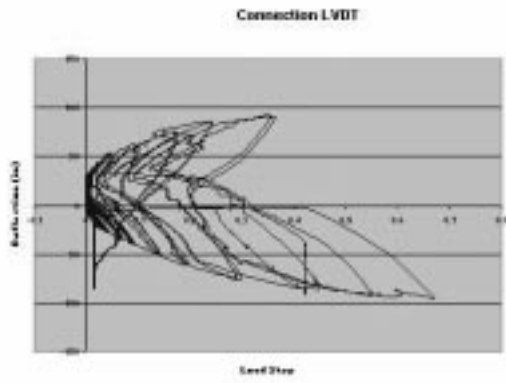


Figure 59.

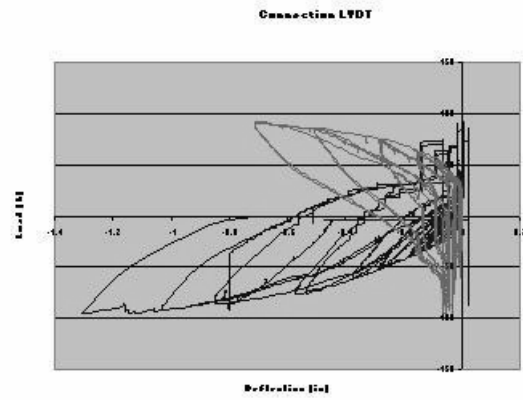


Figure 60.

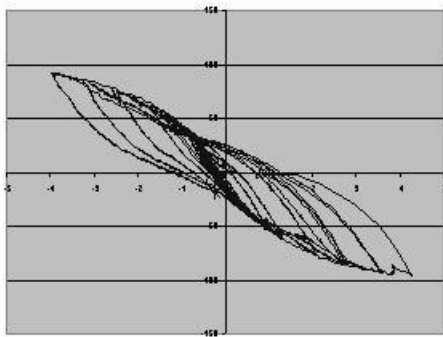


Figure 61.

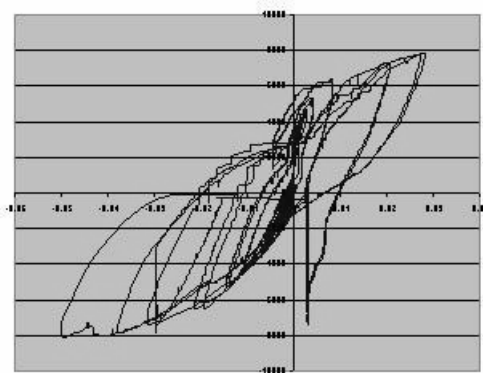


Figure 62.

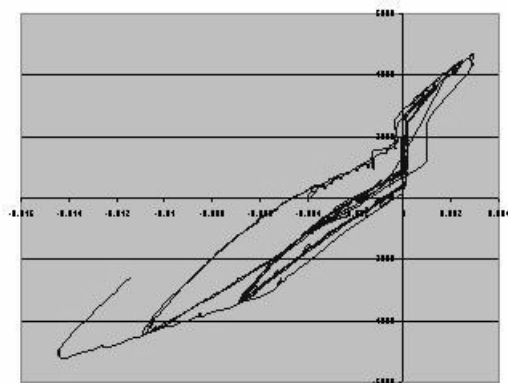


Figure 63.

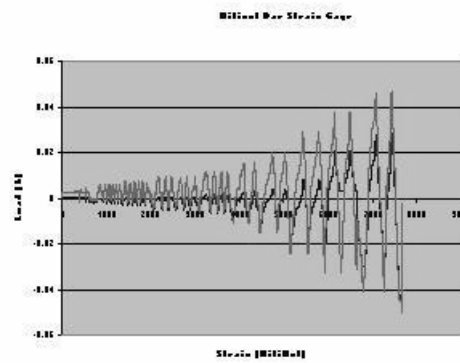


Figure 64.